Electrostatic Micromechanical Actuator with Extended Range of Travel

Edward K. Chan and Robert W. Dutton, *Fellow, IEEE*

Abstract—The practical design issues of an electrostatic micromechanical actuator that can travel beyond the trademark limit of conventional actuators are presented in this paper. The actuator employs a series capacitor to extend the effective electrical gap of the device and to provide stabilizing negative feedback. Sources of parasitics—from layout and two—dimensional nonuniform deformation—that limit the actuation range are identified and their effects quantified. Two "folded capacitor" designs that minimize the parasitics and are straightforward to implement in multiuser microelectromechanical processes are introduced. The effects of residual charge are analyzed, and a linear electrostatic actuator exploiting those effects is proposed. Extended travel is achieved in fabricated devices, but is ultimately limited by tilting instabilities. Nevertheless, the resultant designs are smaller than devices based on other extended-travel technologies, making them attractive for applications that require high fill factors. [512]

Index Terms—Electromechanical actuator, extended travel, folded capacitor, parasitics, residual charge, stability, tilt.

I. OVERVIEW

MICROMECHANICAL electrostatic actuators typically have a travel range limited to one-third to one-half of the initial gap. A method or mechanism to extend that travel range, preferably to the extent of the entire initial gap, is highly desirable, especially for optical applications. Such a method will increase the tunable range of an optical device such as a micromechanically tuned laser [1]. This method will also enable the continuous analog control of a positioner instead of the limited on-off behavior that avoids teetering near the threshold of instability.

Several methods have been suggested that extend the usable range of electrostatic actuators, including closed-loop voltage control [2], series feedback capacitance [3]–[5], and "leveraged bending" [6]. Leveraged bending is the simplest method of the three, requiring that the electrostatic force be applied between the fulcrum (typically the anchor) and the segment of the beam that should be deflected. Mechanical advantage and increased device area are traded off for the increased range of motion. The closed-loop controller is much more complicated—requiring accurate and fast monitoring of the position of the movable element and feedback control circuitry to stabilize the system in the

unstable regime. No fabricated devices have been demonstrated to date. The series feedback capacitance method introduced by Seeger *et al.* employs a capacitor in series with the electrostatic actuator to extend the effective electrical gap of the actuator. That way, the movable element can travel up to one-third of the new effective gap, which is larger than the entire initial gap of the original actuator. The concept is simple and the resultant device is compact—not any larger than a conventional device—but the practical design issues, neglected in [3]–[5], require attention.

In this paper, the realistic design issues involved in designing a full-gap positioner are presented along with measurements of fabricated devices and analyses of their performance. After introducing the theory of operation of the device, the effects of parasitic capacitances, both from layout and from operation, are discussed. A "folded capacitor" structure is introduced that limits parasitics, is easy to fabricate in multiuser microelectromechanical processes (MUMPs) [7, [Online.] Available: http://mems.mcnc.org/mumps.html], and does not take up much more die area than a conventional device. The first measurements of an electrostatic actuator incorporating a series capacitor are presented. The actuator can travel beyond the conventional limit, but is ultimately limited by tilting instabilities. This instability is analyzed further and shown to potentially be a fundamental limit to performance.

II. SERIES CAPACITOR FEEDBACK

Fig. 1(a) shows a schematic of a conventional electrostatically actuated micromechanical actuator. The movable electrode moves under voltage control up to one-third of the initial gap. If actuated beyond that threshold, the movable electrode snaps down onto the bottom electrode. If the goal is to achieve a travel range of g_0, then the initial gap can be extended to $3g_0$, as shown in Fig. 1(b), to have a stable region of up to g_0. This design, however, is not very satisfactory because it requires a large gap that can be difficult to fabricate. Noting that this configuration is actually two capacitors in series, the additional $2g_0$ gap can be replaced with an equivalent series capacitor as shown in Fig. 1(c). The electric field configuration is maintained; hence, the movable plate can traverse the entire g_0 gap stably. The voltage required to actuate the movable plate increases with the addition of the series capacitor because the total initial effective electrical gap is three times as large as the original. Since actuation voltages scale to the 3/2 power of the gap, the voltages increase by at least a factor of five. Methods to reduce these voltages using MOS capacitors were proposed in [3]–[5]. Since the additional gap must be at least twice the

E. K. Chan was with the Center for Integrated Systems, Stanford University, Stanford, CA 94305 USA. He is now with Bell Laboratories, Lucent Technologies, Murray Hill, NJ 07974 USA.
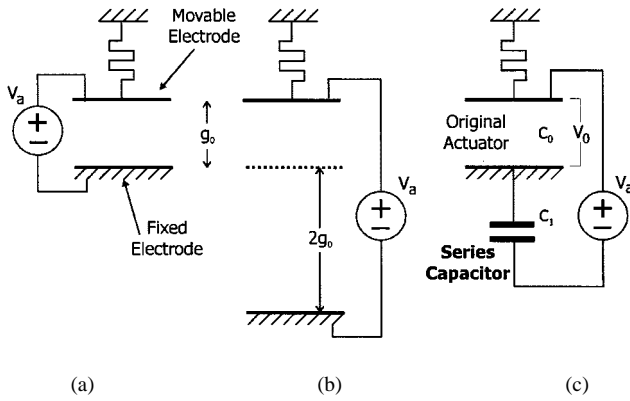R. W. Dutton is with the Center for Integrated Systems, Stanford University, Stanford, CA 94305 USA.

Fig. 1.   Electrostatic micromechanical actuator. (a) Conventional actuator with limited range of travel. (b) Actuator with extended gap and, hence, extended range of travel. (c) Actuator with series capacitor that is equivalent to design in (b). The series capacitor and original actuator form a voltage divider that provides negative feedback to stabilize the system.

original gap for stable full-gap travel, the equivalent series capacitance must be less than one-half the initial capacitance of the original actuator c_0^i. The idea is simple, but the challenge is to maintain the simplicity in the face of nonidealities.

The original actuator and series capacitor form a voltage divider circuit. As the movable electrode approaches the fixed electrode, the capacitance of the actuator increases, thus decreasing the fraction V_0 of the total applied voltage V_a, which is imposed across the actuator according to

$$V_0 = \frac{c_1}{c_0 + c_1} V_a \qquad (1)$$

where c_0 is the variable capacitance of the original actuator and c_1 is the series capacitance. When the movable electrode goes beyond one-third of the original gap, the rapid increase in capacitance provides the negative feedback necessary to stabilize the actuator so it can traverse the entire gap stably. Initially, V_0 increases with V_a, with the rate of increase decreasing as c_0 increases, as indicated by (1). Beyond one-third of the initial gap where V_0 equals the original V_{pi}, V_0 actually starts to decrease since c_0 increases rapidly in this region, thus providing negative feedback. As the movable plate approaches the fixed plate, the capacitance c_0 goes toward infinity and V_0 goes toward zero. The electrostatic force remains finite, however, since the electrostatic force is inversely proportional to the square of the gap, which also goes toward zero. At all times, the mechanical and electrostatic forces are balanced and the system is stable.

III. PARASITIC CAPACITANCES

A. Parasitics from Layout

The cross section of a typical electrostatically actuated device fabricated in MUMPs is shown in Fig. 2(a). c_0 and c_1 are the intrinsic or desired device capacitances, whereas c_{p1}, c_{p2} and c_{p3} are parasitics. c_{p2} and c_{p3} are typically large because the dielectric layer is electrically thin. Depending on whether the substrate is left floating or grounded, the parasitic capacitances can be in parallel with either c_0 or c_1. The configuration of Fig. 1(c) can be generalized to the circuit of Fig. 2(b), which includes parasitic capacitances. Here, c_1 includes parasitics formerly in parallel with the desired series capacitance. c_3 is not important to
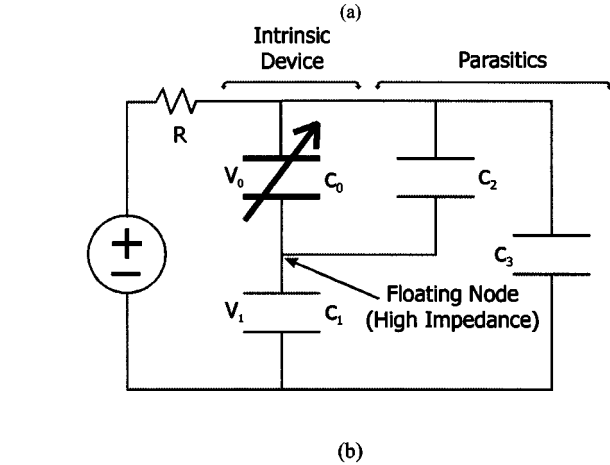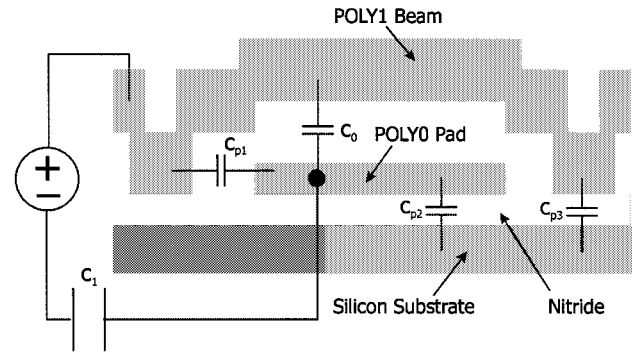

Fig. 2.   (a) Cross section of a typical electrostatically actuated device designed for MUMPs. Large parasitic capacitances are connected to the POLY0 pad. (b) Circuit of actuator with series capacitor, augmented by parasitic capacitances in parallel and in series with the variable capacitor.

static behavior since it is driven directly by the voltage source, but it will affect dynamics.

The expressions describing the static behavior of the actuator in the presence of a series feedback capacitor and parasitic capacitors can now be derived. Let

$$c_0 \propto \frac{1}{g_0 - u} \qquad c_1 \propto \frac{1}{ng_0} \qquad c_2 \propto \frac{1}{mg_0} \qquad (2)$$

where g_0 is the desired travel range, u is displacement, and m and n are positive constants. The voltage across c_0 is determined by the capacitive voltage divider in Fig. 2(b) to be

$$V_0 = \frac{c_1}{c_0 + c_1 + c_2} V_a = \frac{m(g_0 - u)}{(m+n)(g_0 - u) + mng_0} V_a. \qquad (3)$$

The sum of the electrostatic and mechanical forces gives the total equilibrium force on the movable electrode

$$F_t = -ku + \frac{\varepsilon A}{2(g_0 - u)^2} \left[\frac{m(g_0 - u)}{(m+n)(g_0 - u) + mng_0} V_a \right]^2 = 0. \qquad (4)$$

Differentiating this expression with respect to u to determine the point at which the equilibrium solution becomes unstable gives

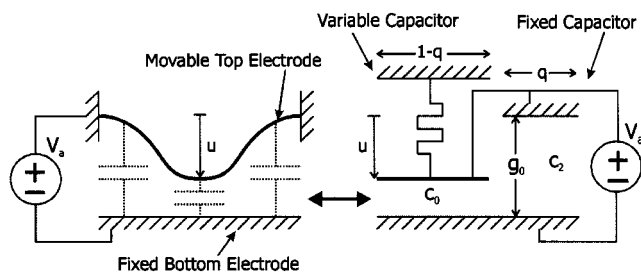$$u_{\max} = \frac{g_0}{3} \frac{m + n + mn}{m + n} \qquad (5)$$

Fig. 3.   Ideal 2-D beam with nonuniform displacement and its two-lump equivalent (variable + fixed capacitor).

as the maximum stable displacement of the movable electrode as a function of m and n. In the limit as $m \to \infty$ (no parasitic capacitor in parallel with c_0)

$$u_{\max} \to \frac{g_0}{3}(1+n) \tag{6}$$

implying that n should be larger than two for full gap travel $(u_{\max} \to g_0)$, as noted previously. As $n \to \infty$ (infinitely small series capacitor for maximum feedback and stability)

$$u_{\max} \to \frac{g_0}{3}(1+m) \tag{7}$$

implying that c_2 must be no larger than $c_0^i/2$ if full gap travel is to be achieved. Thus, the electrostatic positioner must have well-controlled capacitances and parasitics.

B. Parasitics from Deformation

Another source of "parasitics" arises from the deformation of a beam in two dimensions. When the beam in Fig. 2 deforms, the displacement of the center portion is largest whereas the portions near the step-up supports hardly move at all. This two–dimensional (2-D) nonuniform displacement is a subtle, but significant source of parasitic capacitance in parallel with the intrinsic device. The 2-D beam/capacitor can be modeled as the sum of two one–dimensional (1-D) capacitances—a variable capacitor in parallel with a fixed capacitor, as shown in Fig. 3. The total capacitance can be expressed as

$$c = c_0 + c_2 \propto \frac{1-q}{g_0 - u} + \frac{q}{g_0} \tag{8}$$

where c_0 and c_2 represent the same elements as in Fig. 2(b), and q is a proper fraction that increases as u, the center displacement, increases. The larger the value of q, the more significant the effect of the parasitic fixed capacitance.

Fig. 4(a) shows the normalized simulated capacitances of several 2-D 400-μm-long electrostatically actuated beams. These coupled electromechanical simulations were performed in Matlab [8]. The beams are 2-μm thick and are suspended 2-μm above a ground plane—the nominal dimensions of a MUMPs device. The Young's modulus is 140 GPa, whereas the uniaxial residual stress is a compressive 6 MPa. The 2-D capacitances are normalized to the capacitance of an ideal 1-D parallel-plate capacitor, whose gap is equal to the distance between the center of the 2-D beam and ground plane. As shown, the capacitances of the 2-D devices are only fractions of the 1-D device as the center of the beam approaches the ground plane. If the length of the fixed bottom electrode under the 2-D
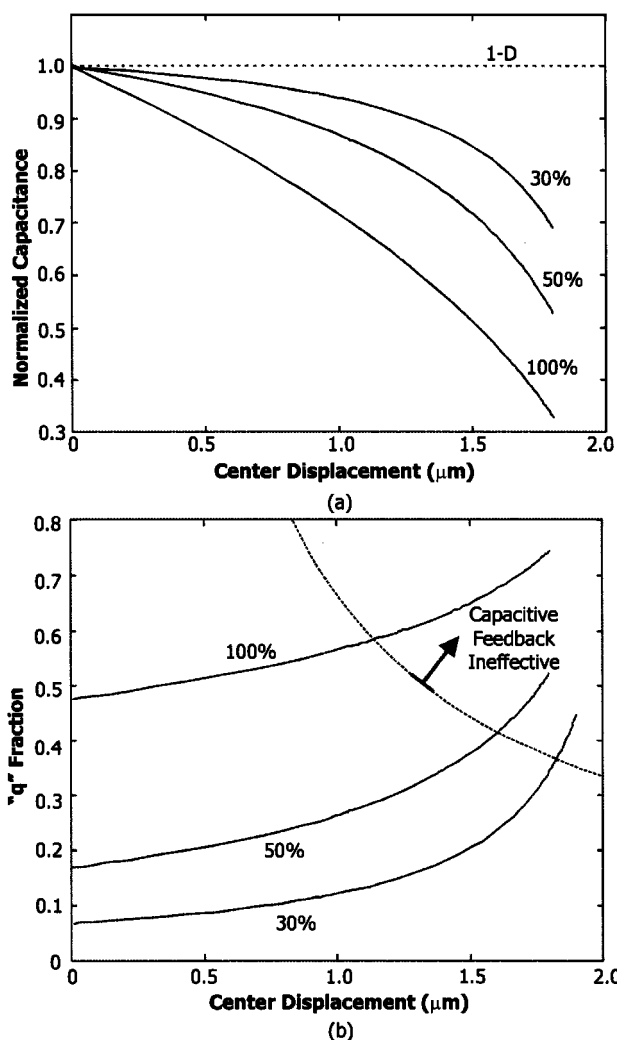

Fig. 4.   (a) Capacitance of 400-μm-long beams as a function of displacement, normalized to the capacitance of a 1-D device with displacement equal to the displacement of the beam center. The labels indicate the length of the bottom actuating electrode as a fraction of the upper beam length. (b) q-fraction as a function of displacement, computed from the capacitances in (a). Capacitive feedback is ineffective for displacements with q-fractions above the dotted line.

beam is reduced (as a percentage of the beam length), the 2-D device approaches 1-D-like behavior because the deformation is more uniform over the more limited center region.

q is computed from the capacitance-displacement curves of Fig. 4(a) using (8) and plotted in Fig. 4(b) as a function of center displacement u, and parameterized by bottom electrode length. The shorter the bottom electrode, the more 1-D-like the behavior of the system and, hence, the smaller the value of q. q increases as the displacement increases because the diminishing gap amplifies the lack of flatness of the deformed beam. According to (2), the ratio of the variable capacitance to the fixed capacitance c_0/c_2 is $mg_0/g_0 - u$. Equating this with the same ratio obtained from (8) gives m in terms of q

$$m = \frac{1-q}{q} \tag{9}$$

which, when inserted in (7), gives

$$u_{\max} = \frac{g_0}{3q}. \tag{10}$$

Plotting $q = (g_0/3u)$ in Fig. 4(b) gives the maximum q allowed for the desired range of motion u. The displacement at the intersection of this line with the previous q–u curves indicates the maximum achievable stable travel. Beyond that, q is too large, i.e., the parasitic is too large for effective stabilization. This assumes that the mechanical restoring force as used in (4) is still linear with displacement, which is not true in real life due to stress-stiffening effects. Nonlinear stress stiffening actually increases the range of stable travel, even without capacitive stabilization, to about one-half of the initial gap, up from the one-third of the linear case. Thus, all the 2-D devices shown in Fig. 4 are stable up to about 1 μm of displacement. Beyond that, capacitive feedback can stabilize the device until the increasing displacement causes q to increase to the limit indicated by the dotted line. For example, for the device with a bottom electrode that is 30% of the upper electrode length, capacitive feedback will allow stable travel up to 1.8 μm or 90% of the 2-μm gap. This, according to (7), assumes an infinitely small series feedback capacitor—a larger capacitor will reduce the stable travel range. The parasitics due to the nonuniform deformation of cantilevers is even more severe than for fixed–fixed beams. Clearly, 2-D-like behavior must be avoided.

IV. RESIDUAL CHARGE

Residual charge can accumulate in electrostatically actuated devices containing electrically isolated nodes such as the node between the original actuator and the series capacitor [see Fig. 2(b)]. Such charge, due to charging in dielectrics, for example, shifts the electrostatic forces by a voltage offset, which scales according to the amount of charge [9]. This causes the displacement of the positioner to drift over time if charge accumulates. Actuation characteristics vary significantly from measurement to measurement if the top beam or centerpiece comes into contact with the underlying electrode. A high-impedance switch that can reset the voltage of the floating node from time to time is very desirable.

If charge lies on a plate that is free to move in an electric field, the effect is more involved. One possible configuration could consist of a movable precharged floating conductor, like an electret foil, inserted between two voltage-driven plates. The electrostatic pressure on the floating conductor—the product of charge on the conductor and the average of the electric fields on both sides of the conductor—is now

$$P_{\text{electrostatic}} = \rho \left[\frac{V_a}{d_1} - \frac{\rho}{\varepsilon} \left(\frac{d_2 - u}{d_1} - \frac{1}{2} \right) \right]. \quad (11)$$

ρ is the areal charge density on the floating conductor, V_a is the voltage applied between the plates, d_1 is the distance from the first plate to the floating conductor, d_2 is the distance of the second plate to the same floating conductor, ε is the permittivity of the gap, and u is displacement. This electrostatic force is linear with voltage and displacement. Since the conventional inverse square behavior is absent, there is no abrupt pull-in effect, and actuation is always stable, potentially allowing for stable and linear electrostatic actuation. The main design issues are imparting a precharge to the floating node and then maintaining its electrical isolation. Parasitic capacitances affect lin-
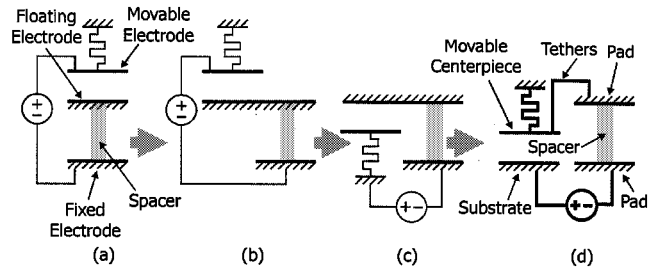

Fig. 5. Transformation of three-conductor stack into side-by-side configuration. (a) Original straightforward three-conductor stack. (b) Floating electrode is elongated to separate variable capacitor from series capacitor. (c) The left-hand side is folded over to place the capacitors side by side. (d) The movable portion is flipped back on top to get the final two-conductive-layer configuration.

earity and the stable range of travel. This design is practically impossible in MUMPs, but might be achievable in silicon on insulator (SOI)-based micromachining processes.

V. FOLDED CAPACITOR DESIGN

Fabricating a device based on a straightforward implementation of the actuator with a series feedback capacitor, as shown in Fig. 5(a), would require a dielectric spacer many times the thickness of the travel gap to maintain the proper ratio. This device cannot be realized in MUMPs. The desired configuration is Fig. 5(d), where the series capacitor is alongside the original actuator, not stacked underneath it. The series capacitor is connected to the actuator by flexible tethers. Fig. 5(b) and (c) conceptualizes the transformation of the initial three conductor stack [see Fig. 5(a)] into the equivalent two-layer design more suitable for surface micromachining. First, the floating conductor/electrode is extended, as shown in Fig. 5(b), so that the moving elements and the series capacitor can eventually be placed side by side. The electric-field configuration is maintained because the floating electrode is an equipotential. Next, the left-hand side is folded over the floating electrode, creating the "folded capacitor" configuration of Fig. 5(c). By doing so, the original actuator is now alongside the series capacitor, thus requiring only two conductive layers instead of the original three-layer stack, while maintaining low parasitic capacitances. The actuated part must now be put back on top to be free to move. To get to the final configuration, the electrical connections are maintained, while the mechanical elements on the left-hand side are swapped. The electrostatic force configuration on the movable electrode in Fig. 5(d) is exactly the same as that in the initial design of Fig. 5(a). No additional parasitics were introduced, and this two-conductive-layer configuration can be translated directly into a MUMPs design.

Profiles of two designs fabricated in MUMPs are shown in Fig. 6(a) and (b). The essential elements of the designs are labeled corresponding to Fig. 5(d). The profiles match the simple 1-D schematic of Fig. 5(d) closely, with the main difference being that the actual physical device has tethers on each side of the centerpiece to help maintain balance and symmetry. The device consists of a nominally rigid centerpiece fabricated in POLY1 suspended by tethers of either POLY1 or POLY2. These designs are not much different from a conventional actuator shown in Fig. 2(a), except for the addition of dielectric spacers
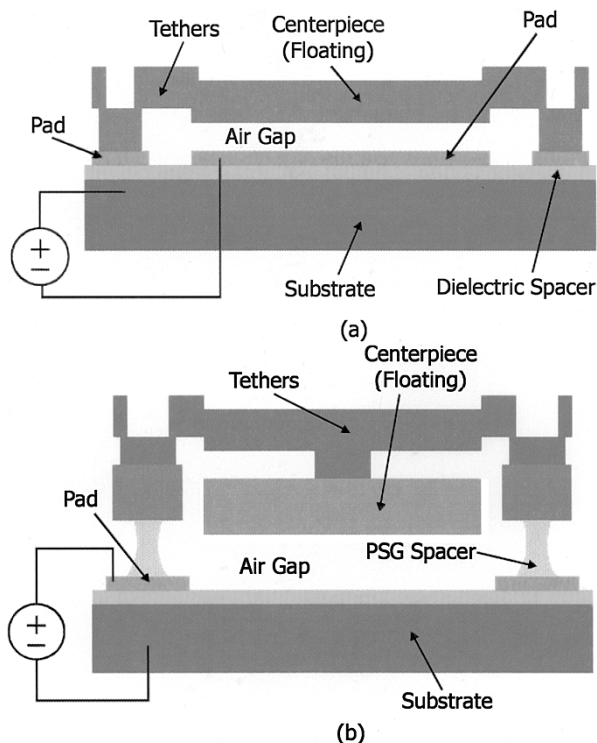
Fig. 6. Cross sections of folded capacitor structures. (a) Structure using the nitride layer as the dielectric spacer. Centerpiece and tethers are made from POLY1. (b) PSG forms the dielectric spacer after a controlled HF etch. The tethers, made from POLY2, are shielded from the substrate electrode by the centerpiece, thus reducing parasitics.
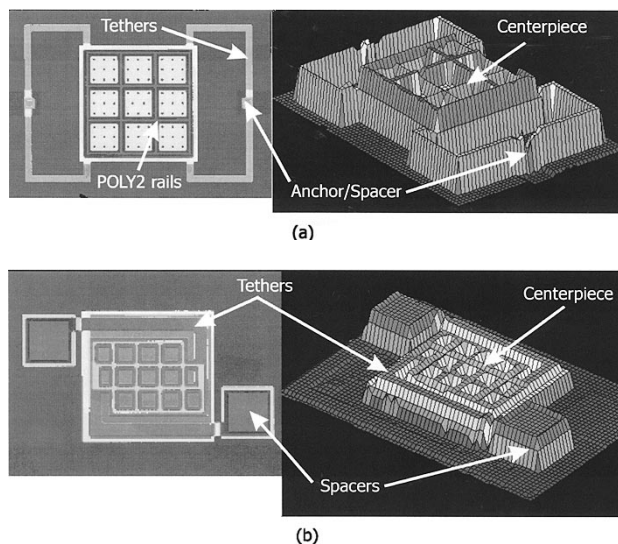

Fig. 7. Interferometric views of folded-capacitor designs. The images on the left–hand side are top views, whereas the images on the right–hand side are 3-D views. Interferometry only provides the shape of the top surface so the sacrificial gap and other underlying structures are not visible. (a) POLY1 is used for both the centerpiece and tethers. Nitride forms the spacer. (b) POLY2 forms the tethers, which are shielded from the bottom electrode to minimize parasitics. PSG forms the spacer.

under the tether anchors. The gap between the POLY1 centerpiece and POLY0 pad was reduced with a dimple etch, as shown in Fig. 6(a), to increase c_0^i and, hence, relax the constraints on achieving the desired high capacitance ratio c_0^i/c_1. Small series capacitors c_1 are difficult to design in the MUMPs process because the dielectrics are electrically thin.

In the Fig. 6(a) design, the series capacitor is formed by the POLY0 pad under the anchor and silicon substrate, sandwiching the nitride. The actuator capacitance, c_0, is between the POLY1 centerpiece and POLY0 pad directly beneath it. The tethers are formed in POLY1 and have parasitics associated with nonuniform deformation similar to that described in Section III-B. For the design of Fig. 6(b), a controlled HF etch of the sacrificial phosphosilicate glass (PSG) creates dielectric spacers, which form the series capacitors and electrically isolate the tethers and centerpiece, leaving them floating. The actuator capacitance is between the centerpiece and the silicon substrate. The POLY2 tethers are shielded from the substrate by the POLY1 centerpiece thus reducing associated parasitics.

Top and three-dimensional (3-D) views of these two designs are shown in the Zygo New View 200 surface profiler images of Fig. 7. The movable centerpieces are large compared to the areas of the series capacitors due to the constraints of the thin MUMPs dielectrics. The centerpieces range from 140 μm × 140 μm to 260 μm × 260 μm. In Fig. 7(a), the series capacitors at the anchors are very small, only 23 μm × 25 μm, because the nitride is electrically thin. The capacitance ratios c_0^i/c_1 for these devices range from 1.5 to 8.1. A ratio larger than two is required for full-gap travel. The tethers are designed with flex-

ures for maximum compliance to compensate for the increase in actuation voltage due to the addition of the series capacitor. The flexures also provide stress relief to prevent buckling. POLY2 rails are deposited on the POLY1 centerpieces to help maintain flatness during actuation that is essential to the proper operation of these devices. The structure in Fig. 7(b) uses PSG as the dielectric spacer for the series capacitors, and POLY2 as tethers. The series capacitors have larger area than those in Fig. 7(a) because the PSG is thicker than the nitride. This design requires careful control of the PSG etch in HF. The undercut of PSG in HF is roughly 30 μm per minute. Square POLY1 pads with edges of 80 μm or 110 μm were designed to form the series capacitors. The capacitances of these series capacitors were computed assuming some mixture of air and PSG dielectrics under the POLY1 pads resulting from an undercut of exactly 30 (1-min etch) or 45 μm (1.5-min etch). The capacitance ratios for this range of devices were designed to be between 1.3–7.2.

VI. PERFORMANCE

The performance of several permutations of folded capacitor structures fabricated in the MUMPs 29 run were analyzed under the Zygo interferometer. After a 1-min HF etch, most of the large centerpieces were still not released because the HF could not undercut the PSG through the arrays of 3 μm × 3 μm etch holes. Thus, dies released in a 1.5-min etch were used, but even then, some dies had unreleased parts. Measurements of the device shown in Fig. 7(a) are shown in Fig. 8(a). The first curve actually shows the performance of a conventional actuator. The measurement was made on exactly the same structure, except that the electrical probes bypassed the series capacitor. One probe was positioned at the top center of an anchor/series capacitor, making sure that the rest of the structure was not perturbed. The plot of the normalized displacement of the centerpiece as a func-
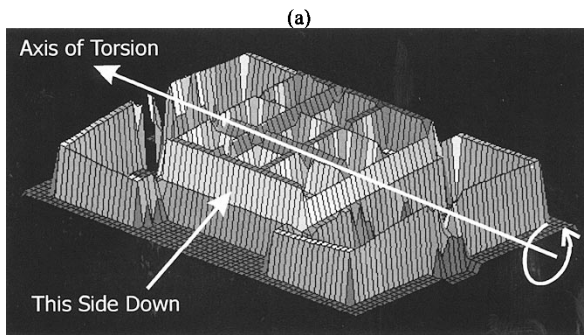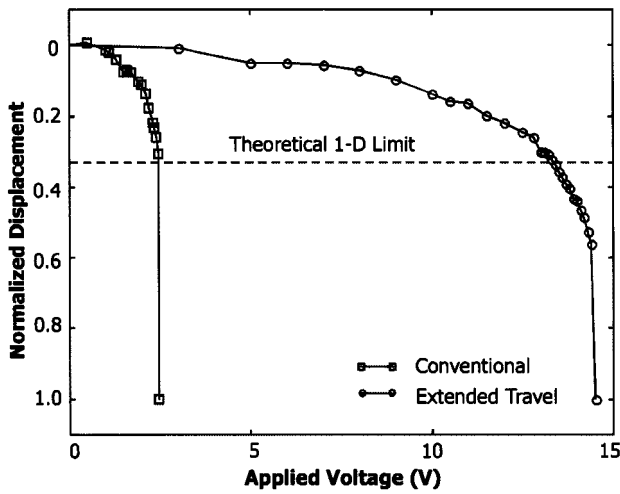
Fig. 8. (a) Measured displacement-voltage characteristic of a conventional actuator, and an actuator with extended travel. Both measurements were made on the same device—the measurements of a conventional actuator were obtained by bypassing the series capacitance with the probes. Displacement shown is that of the center of the centerpiece. (b) Surface profile of a folded capacitor device tilted at pull-in. A preferred axis of torsion exists, spanning the two anchors.

Fig. 9. (a) Rigid-body model of actuator with series capacitor. The torsional degree of freedom is introduced to analyze effects of asymmetry between the right- and left-hand-side tethers. (b) Profile of centerpiece as the actuation voltage is increased. The left-hand-side tether is 10% stiffer than the right-hand-side tether. Labels are of applied voltage. The last three profiles are essentially at the same voltage, indicating a sharp descent due to tilting.

tion of voltage shows that the actuator travels up until the theoretical limit, then collapses to the bottom. The measurements match theory because the mechanical stiffness of the slender tethers is linear with displacement. The actuator with the series capacitor can go beyond the theoretical limit, almost twice the conventional range, before collapsing. The increase in actuation voltage confirms that the fundamental principles of capacitive voltage division and negative feedback are operational.

Further analyses reveal that pull-in still occurs, even though the designed capacitance ratio is sufficient, because tilting occurs. 1-D-like behavior should be maintained at all times for proper operation, but asymmetry in the device causes tilting to occur, as shown in Fig. 8(b). As the centerpiece deflects beyond the conventional theoretical limit, any asymmetries are amplified. When one side of the plate deflects more than the other, the capacitance change due to this tilting is insufficient to adjust the voltage of the plate to maintain stability. Electrostatic forces concentrate on that side of the plate causing positive feedback, which snaps that side down. This tilting was observed on all the other folded capacitor designs at travel ranges close to that shown in Fig. 8(a).
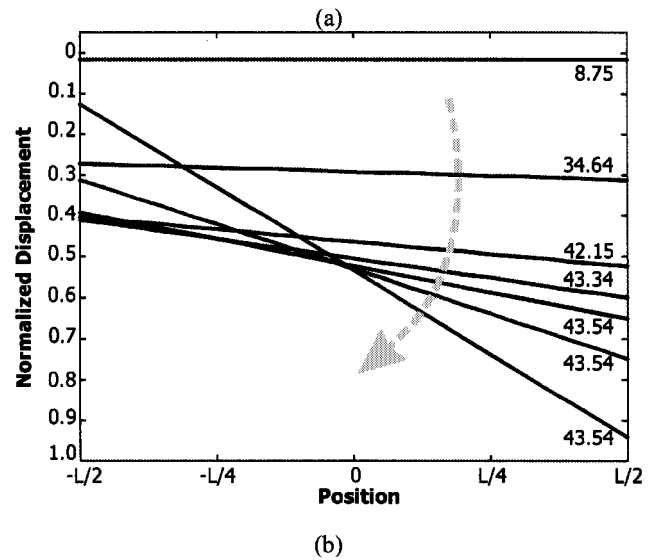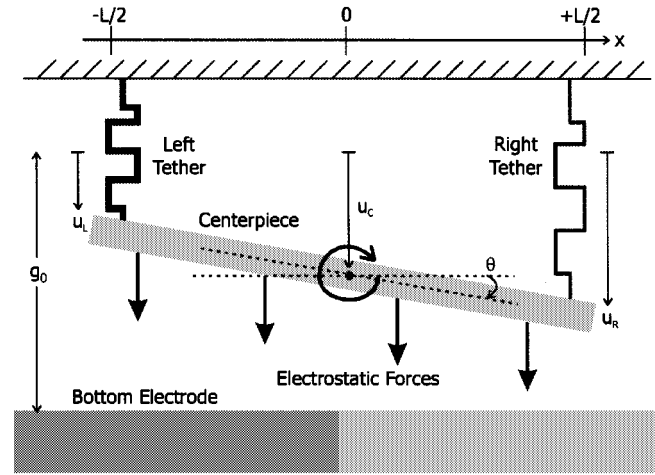
VII. TILTING

This tilting phenomenon was analyzed in two-dimensions using rigid body simulations. The model consists of a rigid centerpiece suspended by tethers at the ends, as shown in Fig. 9(a). The equations of motion that describe the centerpiece are

$$m\frac{d^2 u_C}{dt^2} = -k_L u_L - k_R u_R + \frac{W\varepsilon_0 V^2}{2} \int_{-(L/2)}^{L/2} \frac{dx}{[g_0 - u(x)]^2} \tag{12}$$

for the vertical displacement of the center and

$$I\frac{d^2\theta}{dt^2} = \frac{L}{2}k_L u_L - \frac{L}{2}k_R u_R + \frac{W\varepsilon_0 V^2}{2} \int_{-(L/2)}^{L/2} \frac{x\,dx}{[g_0 - u(x)]^2} \tag{13}$$
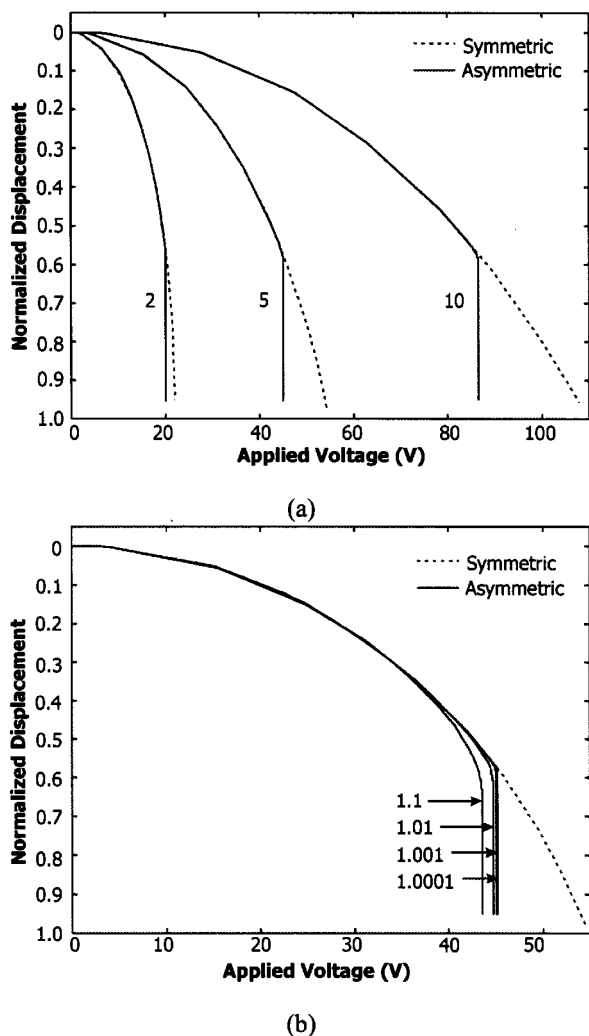
Fig. 10. Normalized displacement of the centerpiece as a function of applied voltage, showing the range of travel that can be achieved. The displacement shown is the maximum displacement, which is of the right-hand side of the centerpiece. (a) The labels are the original-to-series capacitance ratios. At close to a normalized deflection of 0.6, asymmetry causes the devices to tilt and snap down. The ranges of travel do not seem to depend on the ratio of the capacitances. (b) Displacement for devices with different degrees of asymmetry. The four labeled curves correspond to the cases where the tether on the left-hand side is stiffer by 10%, 1%, 0.1%, or 0.01%. For asymmetries resolvable by the simulation tolerance, the device tilts and pulls in close to a normalized displacement of 0.6. The capacitance ratio is five in all cases.

for the rotation of the centerpiece. In the numerical simulation, the centerpiece is discretized into small segments. Damping terms are added to help quasi-static simulations converge quickly. For the centerpiece, m is the mass, I is the moment of inertia, W is the width, and L is the length. k_L and k_R are the stiffnesses of the left- and right-hand-side tethers, respectively. Asymmetry is introduced by increasing the relative stiffness of the left-hand-side tether. The stiffnesses of the tethers are roughly those of 200-μm-long and 30-μm-wide polysilicon beams. Thicknesses, stress, and other properties used are nominal MUMPs parameters. The points at which the tethers attach to the centerpiece are assumed to be perfect pivots that have no resistance to torsion.

Fig. 10(a) shows the simulated quasi-static displacement of an actuator with a series capacitor, as a function of voltage, and

parameterized by capacitance ratio c_0^i/c_1. With perfect symmetry, the actuator can travel the entire gap stably for any capacitance ratio equal to or more than two. With the introduction of a 0.1% asymmetry, the device tilts and pulls in after deflecting close to 60% of the initial gap. This is very close to the measured range of travel. The effect of the degree of asymmetry is investigated in Fig. 10(b). c_0^i/c_1 was fixed at five. Here, all asymmetries that are resolvable within the tolerance of the simulation cause tilting at about 60% of the initial gap. This range of travel does not depend on the ratio of the capacitances or the degree of asymmetry (within the tolerance of the simulation), potentially indicating a fundamental limit to the performance of this technology. The profile of the centerpiece as the actuation voltage is increased is shown in Fig. 9(b). The left-hand-side tether is 10% stiffer than the right-hand-side tether, causing the right-hand side to move down more than the left-hand side. At about 43.54 V, the system becomes unstable and the right-hand side of the centerpiece tilts and pulls in.

The tilting-limited range of stable vertical motion can be obtained analytically by analyzing the vertical and torsional modes separately [10]. Consider the case where the center of the centerpiece is constrained to only rotate and not displace vertically. The capacitance of the actuator is given by

$$
\begin{aligned}
c_0 &= \frac{\varepsilon W}{2} \int_{-(L/2)}^{L/2} \frac{dx}{g - u(x)} \\
&= \frac{\varepsilon W L}{2a} \ln \left(\frac{g+a}{g-a} \right) \\
&\approx \frac{\varepsilon W L}{g} \left[1 + \frac{1}{3} \left(\frac{a}{g} \right)^2 + \frac{1}{5} \left(\frac{a}{g} \right)^4 + \cdots \right]
\end{aligned} \tag{14}
$$

where $a = u(x = (L/2))$ is the vertical displacement of the edge of the centerpiece, and g is the gap at the center of the centerpiece. The expression for capacitance was expanded using the Taylor series expansion

$$
\ln \frac{1+x}{1-x} = 2x + \frac{2x^3}{3} + \frac{2x^5}{5} + \cdots. \tag{15}
$$

To first order, the addition of the series capacitor does not enhance torsional stability because the capacitance and, hence, the voltage across the actuator, does not change as the centerpiece begins to tilt. That is why the capacitance ratio has no effect on stability, as shown in Fig. 10(a).

The torsional equilibrium condition is given by

$$
\tau = kaL + \frac{\varepsilon A L V^2}{8a^2} \left[\ln \frac{g-a}{g+a} + \frac{2ag}{g^2 - a^2} \right] = 0 \tag{16}
$$

where $k = k_L = k_R$, and A is the area of the centerpiece. The term describing electrostatic torque was obtained by evaluating the integral in (13). Taking the derivative of torque with respect to a, setting it to zero, and simplifying the results to obtain the threshold at which the equilibrium becomes unstable gives

$$
-kL - \frac{\varepsilon A L V^2}{4a^3} \left[\ln \frac{g-a}{g+a} + \frac{2ag}{g^2 - a^2} \right] + \frac{\varepsilon A L V^2 g}{2(g^2 - a^2)} = 0. \tag{17}
$$

Using only the first two terms of the Taylor series expansion (15) gives

$$
-kL - \frac{\varepsilon A L V^2}{4a^3} \left[\frac{4a^3 g^2 + 2a^5}{3g^3(g^2 - a^2)} \right] + \frac{\varepsilon A L V^2 g}{2(g^2 - a^2)} = 0. \tag{18}
$$

Taking the limit as $a \to 0$ (centerpiece initially flat, i.e., no tilting) results in the voltage beyond which the centerpiece becomes unstable and tilts

$$V = \sqrt{\frac{6kg^3}{A\varepsilon}}. \tag{19}$$

Applying this voltage in the equation for vertical equilibrium

$$2ku = \frac{A\varepsilon V^2}{2(g_0 - u)^2} = \frac{6k(g_0 - u)^3}{2(g_0 - u)^2} \tag{20}$$

produces the maximum stable vertical range, which is $u = 0.6g_0$, as observed in both measurements and simulations. Note that the critical voltage for the tilting instability depends on the instantaneous gap, which decreases as the voltage increases. This tilting instability can only be observed in devices with series capacitor feedback because conventional devices would snap down vertically prior to this.

The range of motion depends on the ratio of the length of the moment arm to the length of the centerpiece. In this case, where the tethers are attached to the edges of the centerpiece, the range is 60% of the initial gap. If the tethers were attached closer to the center of the centerpiece, the range would be smaller. Conversely, if the effective moment arm were increased by having wide tethers that are resistant to torsion, the stable range would be increased.

VIII. Summary

This paper discussed the practical and realistic design requirements for an actuator with an extended range of travel. The effects of parasitic capacitances from layout and from nonuniform deformation were discussed. Residual charge causes voltage drift, but can also be exploited to create a linear electrostatic actuator. Two "folded capacitor" designs that attempt to meet these practical design challenges were fabricated. Extended travel, almost twice the conventional range, was achieved, but ultimately limited by tilting instabilities. These were the first measurements of devices incorporating series capacitors. Designs using wide tethers would be more tilt resistant and stable. An optimized fabrication process that provides good electrical isolation of nodes will allow more design flexibility. Such designs can be smaller than devices based on other extended-travel technologies, making them attractive for applications that require high fill factors such as micromirror arrays.

References

[1] F. Sugihwo, M. C. Larson, and J. S. Harris, Jr., "Micromachined widely tunable vertical cavity layer diodes," *J. Microelectromech. Syst.*, vol. 7, pp. 48–55, Mar. 1998.
[2] P. B. Chu and K. S. J. Pister, "Analysis of closed-loop control of parallel-plate electrostatic microgrippers," in *Proc. IEEE Conf. Robot. Automat.*, San Diego, CA, May 1994, pp. 820–825.
[3] J. I. Seeger and S. B. Crary, "Stabilization of electrostatically actuated mechanical devices," in *Proc. Transducers'97*, Chicago, IL, pp. 1133–1136.
[4] J. I. Seeger and S. B. Crary, "Analysis and simulation of MOS capacitor feedback for stabilizing electrostatically actuated mechanical devices," in *Proceedings of Microsim II*.   Boston, MA: Comput. Mech., 1998, pp. 199–208.
[5] J. I. Seeger and B. E. Boser, "Dynamics and control of parallel-plate actuators beyond the electrostatic instability," in *Proc. Transducers'99*, Sendai, Japan, pp. 474–477.
[6] E. S. Hung and S. D. Senturia, "Leveraged bending for full-gap positioning with electrostatic actuation," in *Proc. Solid-State Sens. Actuator Workshop*, Hilton Head, SC, June 1998, pp. 83–86.
[7] *MUMP's Design Handbook, Rev. 4*, Cronos Integrated Microsyst., Research Triangle Park, NC, 1999.
[8] E. K. Chan, E. C. Kan, R. W. Dutton, and P. M. Pinsky, "Nonlinear dynamic modeling of micromachined microwave switches," in *IEEE Int. MTT-S Microwave Symp. Dig.*, Denver, CO, June 1997, pp. 1511–1514.
[9] E. K. Chan, K. Garikipati, and R. W. Dutton, "Characterization of contact electromechanics through capacitance-voltage measurements and simulations," *J. Microelectromech. Syst.*, vol. 8, pp. 208–217, June 1999.
[10] E. S. Hung, private communication.

Edward K. Chan was raised in Kuantan, Malaysia. He received the B.S., M.S. and Ph.D. degrees from Stanford University, Stanford, CA, in 1994, 1995 and 1999, respectively, all in electrical engineering.

Before focusing on the characterization of microelectromechanical systems for his dissertation, he developed adaptive feedback systems at the Stanford Linear Accelerator Center, and characterized interconnect performance of multichip modules at MicroModule Systems. He is currently involved with components for wireless and optical communications at Bell Laboratories, Lucent Technologies, Murray Hill, NJ.

Dr. Chan received the 1994 Henry Ford II Award for the highest academic achievement in the School of Engineering, Stanford University.

Robert W. Dutton (S'67–M'70–SM'80–F'84) received the B.S., M.S. and Ph.D. degrees from the University of California at Berkeley, in 1966, 1967, and 1970, respectively.

He is currently the Robert and Barbara Kleist Professor of Engineering at Stanford University, Stanford University, and Director of the Research of the Center for Integrated Systems. His research interests focus on integrated-circuit technologies, especially the use of computational methods.

Dr. Dutton was an editor of the IEEE Transactions on Computer-Aided Design of Integrated Circuits and Systems (1984–1986). He was the recipient of the 1987 IEEE J. J. Ebers Award, the 1988 Guggenheim Fellowship to study in Japan, and the 1996 Jack A. Morton Award. He was elected to the National Academy of Engineering in 1991.